C. R. Mecanique 342 (2014) 417–424

Contents lists available at ScienceDirect

Comptes Rendus Mecanique

www.sciencedirect.com

Separation flow control

Coherent structures in the boundary layer of a flat thick plate

Structures cohérentes dans la couche limite d'une plaque plane épaisse

Bérengère Podvin *, Yann Fraigneau, Christian Tenaud, Virginie Daru

LIMSI-CNRS, BP 133, 91403 Orsay cedex, France

ARTICLE INFO

Article history:
Received 5 September 2013
Accepted 29 November 2013
Available online 3 June 2014

Keywords:
Turbulence
Proper orthogonal decomposition
Separation

Mots-clés :
Séparation
POD
Couplage vitesse–pression

ABSTRACT

We use POD and EPOD (extended POD) analysis to extract the main features of the flow over a thick flat plate simulated with an LES. Our goal is to better understand the coupling between the velocity field and the surface pressure field. We find that POD modes based on the full velocity and energy fields contain both flapping and shedding frequencies. Pressure modes are found to be uniform in the spanwise direction and the most intense variations take place at the mean reattachment point. Velocity modes educed from the pressure modes with EPOD are seen to correspond to eddies shed by the recirculation bubble.

RÉSUMÉ

On considère l'écoulement au-dessus d'une plaque plane épaisse. Nous utilisons la simulation aux grandes échelles et l'analyse POD/EPOD pour comprendre le couplage entre le champ de vitesse et le champ de pression à la paroi. Les modes POD extraits de la vitesse contiennent des fréquences correspondant aux phénomènes de flapping et de shedding. Les modes de pression sont uniformes dans la direction transverse et les variations les plus intenses sont observées au point de réattachement. Les modes de vitesse construits à partir des modes de pression avec l'approche EPOD correspondent à des tourbillons associés à la bulle de recirculation.

1. Introduction

Aerodynamics of vehicles are characterized by the physics of massively separated flows. Kiya and Sasaki [1] showed that the flow in the separation zone is governed by two mechanisms: the shedding of large-scale vortices and a low-frequency unsteadiness called "flapping". The connection between these two mechanisms is still not clear. Another connection that needs to be elucidated is the relationship between the velocity dynamics and the pressure fluctuations. Understanding this coupling represents a challenge for the control of acoustic disturbances. The present paper builds on the results obtained by Tenaud et al. [2] for the LES of the flow over a thick flat plate. We apply POD analysis and EPOD (extended POD) analysis to their numerical data in order to determine the salient features of the pressure and velocity field.

* Corresponding author.
E-mail address: berengere.podvin@limsi.fr (B. Podvin).

http://dx.doi.org/10.1016/j.crme.2014.05.006
1631-0721/

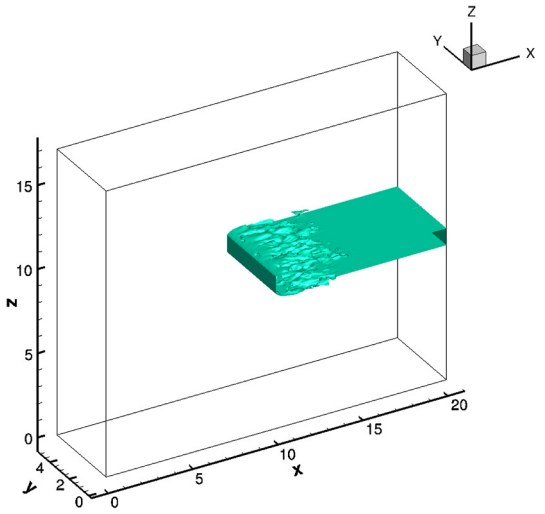

Fig. 1. (Color online) Isosurface of zero streamwise velocity – the arrow indicates the flow direction.

2. The numerical method

We consider the flow over a flat thick plate of thickness H and length L. The total dimensions of the plate in the simulation are $L_x, L_z = (25, 17)H$. The portion of the domain used for POD analysis, which excludes the downstream part of the plate $x > 20H$, is represented in Fig. 1. The height of the numerical domain is $5H$. The Reynolds number based on the constant velocity imposed at the upstream boundary-located at a distance $10H$ from the leading edge of the plate and the plate thickness is $R = 7500$.

The equations of motion are those for a compressible flow. We consider air with a constant specific heat ratio $\gamma = 1.4$. The Prandtl number is taken to be $Pr = 0.73$. The equations are solved using an LES approach. Results reported here were obtained with a dynamic viscosity model [3]. A high-order coupled scheme in time and space was implemented in the parallel code CHORUS. More details can be found in [2].

3. POD analysis

3.1. The POD technique

POD is a statistical technique [4] which extracts the most energetic motions of the flow. Any physical quantity $\underline{q}(\underline{x}, t)$ (which can be the velocity field, density, or any combination thereof) can be written as

$$\underline{q}(\underline{x}, t) = \sum_{n\geq 1} \left(\lambda^n\right)^{1/2} a^n(t) \underline{\phi}_q^n(\underline{x}) \tag{1}$$

where

- the spatial mode $\underline{\phi}_q^n$ is the n-th eigenvector of the eigenproblem

$$\int \langle \underline{q}(\underline{x}, t) \underline{q}(\underline{x}', t) \rangle \underline{\phi}_q^n(\underline{x}') \, \mathrm{d}\underline{x}' = \lambda^n \underline{\phi}_q^n(\underline{x}) \tag{2}$$

  where $\langle \underline{q}(\underline{x}, t) \underline{q}(x', t) \rangle$ is the time-averaged spatial autocorrelation tensor of the quantity $\underline{q}$. By construction the eigenvectors $\underline{\phi}_q$ constitute an orthonormal family;
- λ^n represents the energy of the n-th mode, with $\lambda^1 \geq \lambda^2 \geq \ldots$;
- the temporal coefficient $a^n(t)$ represents the amplitude of the n-th mode and is also normalized to be 1. By construction the coefficients are uncorrelated with each other.

If the autocorrelation tensor is constructed from N selected snapshots of the flow at instants t^k, it can be shown [5] that

$$\underline{\phi}_q^n(\underline{x}) = \sum_{k=1}^{N} \left(\lambda^n\right)^{1/2} a^n\left(t^k\right) \underline{q}\left(\underline{x}, t^k\right) \tag{3}$$

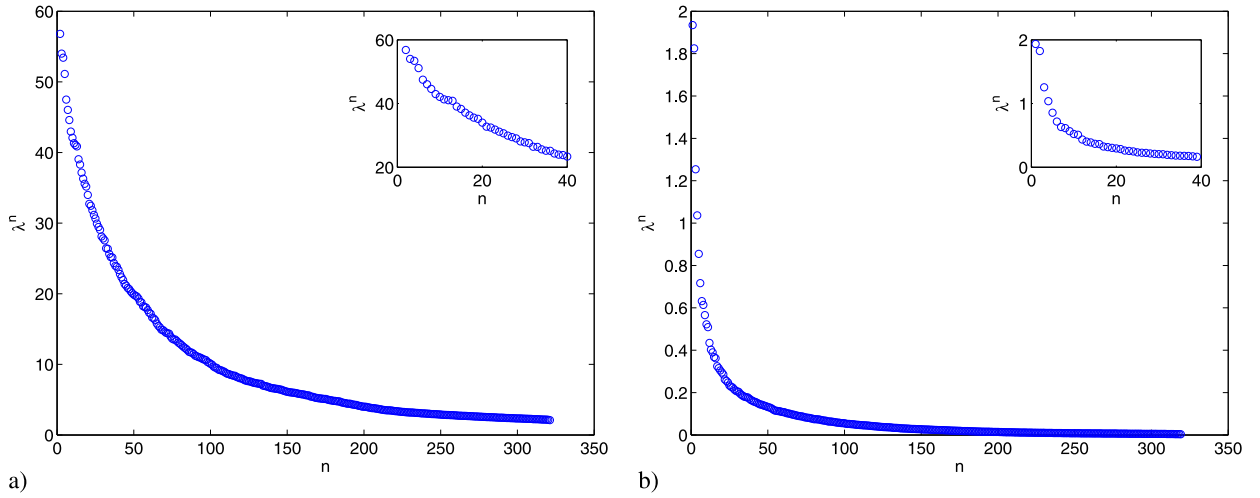

Fig. 2. a) POD spectrum of the full field; b) POD spectrum of the wall pressure.

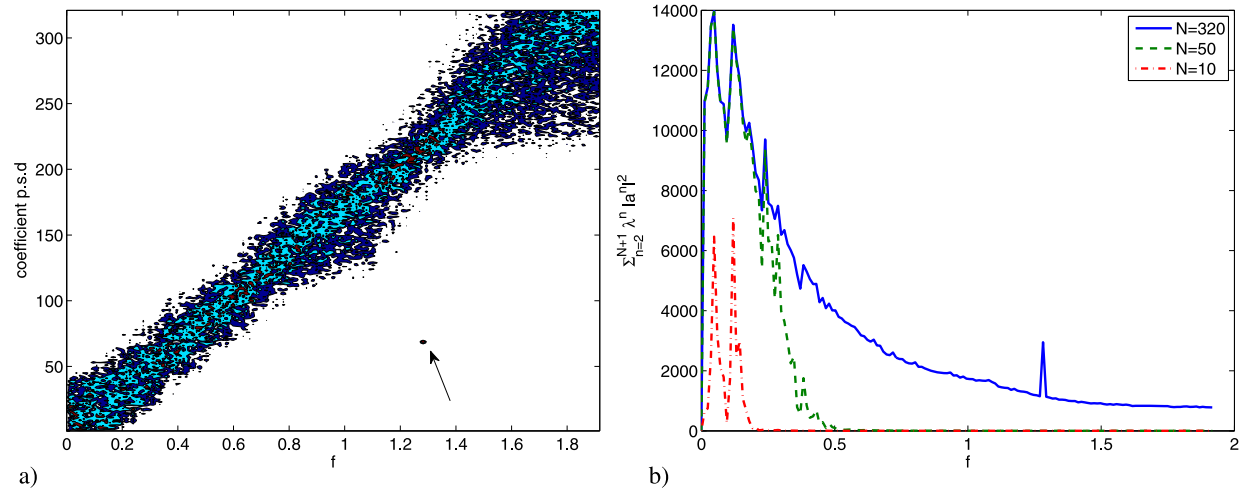

Fig. 3. (Color online) The frequency is adimensionalized with the plate thickness. a) Spectral density of the pressure POD coefficients a_p^n. The arrow indicates the location of the Kelvin–Helmholtz frequency. b) Spectral density of the POD energy $\sum_{n=2}^{N+1} \lambda^n |\hat{a}^n(f)|^2$.

This formulation constitutes the basis of the method of snapshots, which allows the numerical computation of the spatial modes.

POD analysis was applied to the full field $\underline{q} = (\rho, \underline{u}, e)$ over the entire numerical domain as well as to a restriction of the domain below the plate. The nondimensional variables used were the same as the ones in the code (no renormalization or relative rescaling between the different physical quantities was applied). Since the flow is nearly incompressible, the decomposition is essentially equivalent to performing that of the velocity field, so that no rescaling is needed. In any case, it has been shown in the case of thermal convection [6] that rescaling had very little influence on POD results. We also performed POD analysis of the surface pressure field on the bottom surface. In both cases the method of snapshots was used with 320 fields with a time separation of 0.08 time units. The full flow was included in the analysis and its time-average was found to be identical with the first POD mode. The POD energy λ^1 associated with the mean flow is higher than the total fluctuating energy by a factor of 10^6.

3.2. Full-field POD

As shown in [2] a quasi-2D vortex can be distinguished in the recirculation bubble for the mean flow. The height of the vortex is about $0.5H$, where H is the height of the plate and its length is about $2.5H$ – the length of the bubble was about $3.38H$. The recirculation time associated with the vortex was found to be about $20–25H/U_0$, where U_0 is the free-stream velocity. Fig. 2a shows the higher-order eigenvalues $n \geq 2$ when the POD was applied to the full field (over the entire domain). No significant differences were observed when the domain was restricted to the volume below the plate. The relatively slow convergence of the spectrum illustrates the complexity of the flow.

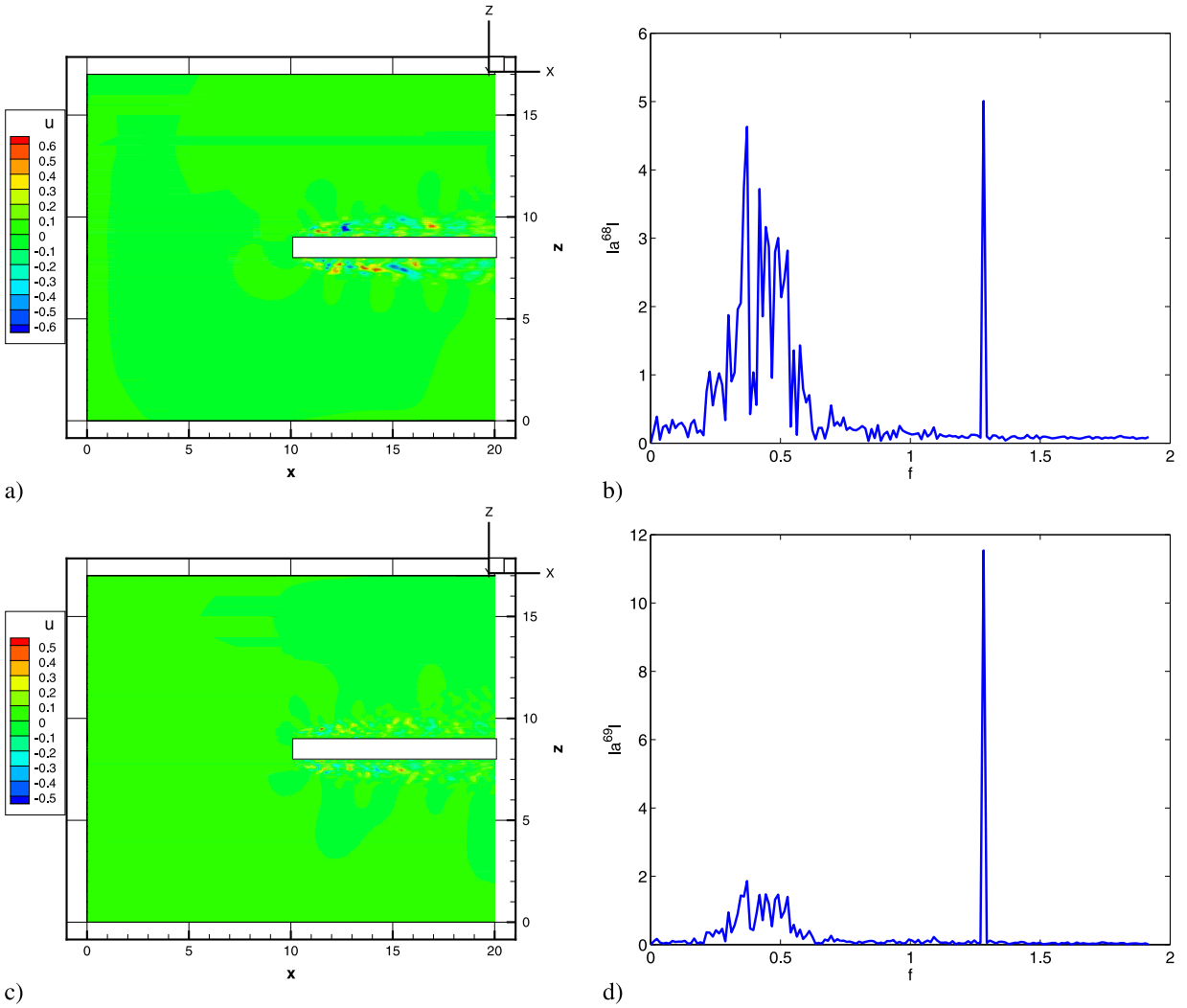

Fig. 4. (Color online) Modes associated with the frequency $fH/U_0 = 1.2$: a) cross-section $y = 0$ of streamwise velocity $\underline{\phi}_u^n$ for $n = 68$; b) spectral density of a^{68}; c) cross-section $y = 0$ of streamwise velocity $\underline{\phi}_u^n$ for $n = 69$; d) spectral density of a^{69}.

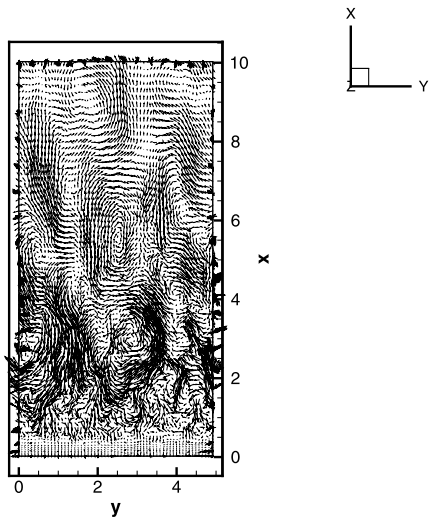

Fig. 5. Horizontal view of the second velocity POD mode at $z = 0.4H$.

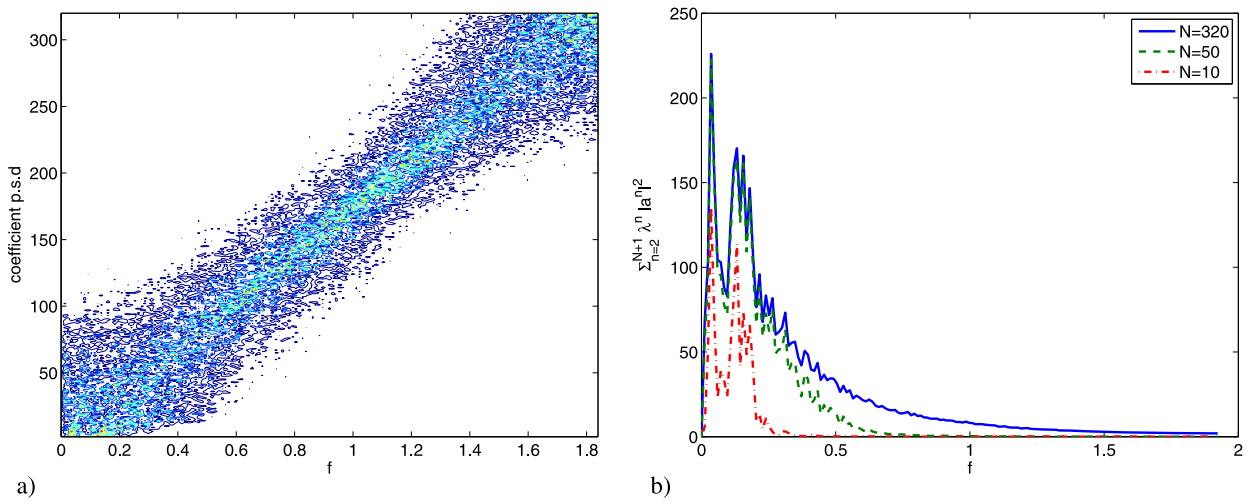

Fig. 6. (Color online) The frequency is adimensionalized with the plate thickness. a) Spectral density of the pressure POD coefficients a_p^n. b) Spectral density of the POD energy $\sum_{n=2}^{N+1} \lambda^n |\hat{a}_p^n(f)|^2$.

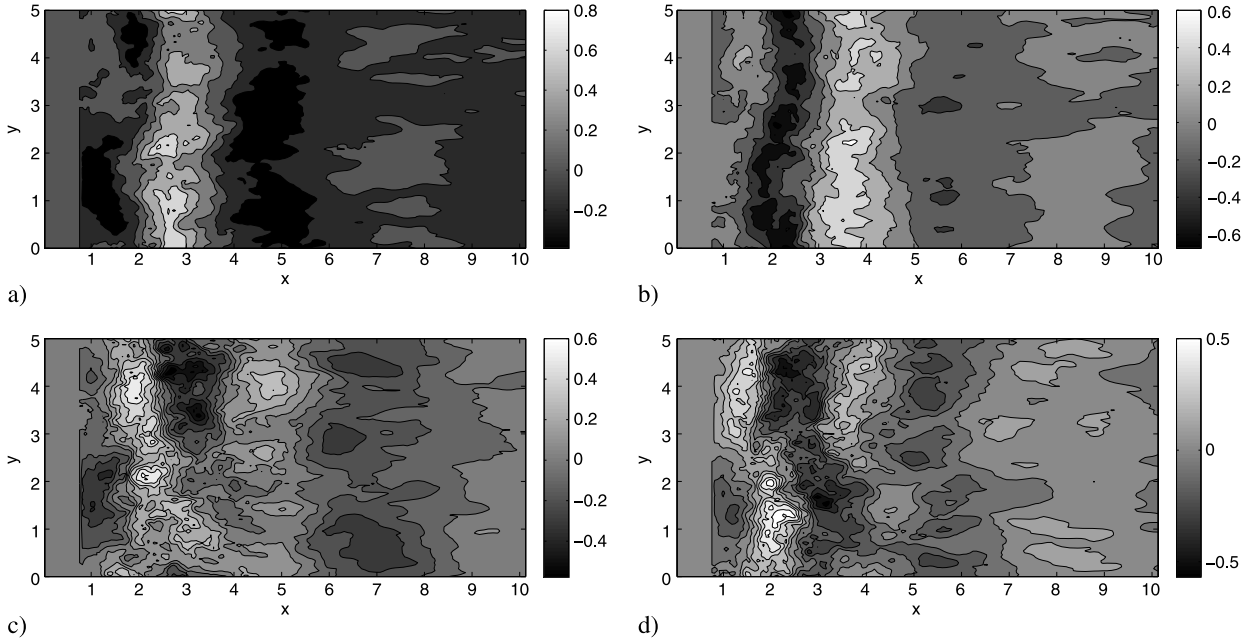

Fig. 7. Pressure POD mode: a) $n = 2$, b) $n = 3$, c) $n = 4$, d) $n = 5$.

The temporal coefficients of the spatial modes were computed and their Fourier transform is represented in Fig. 3. As can be expected higher-order modes are associated with higher frequencies. Fig. 3a shows that the 50 first modes of the full field are characterized by low frequencies $fH/U_0 \leq 0.2$.

Fig. 3b indicates that four peaks can be clearly identified in the total spectrum – one at the frequency of $f_1 H/U_0 = 0.04$–0.05, another at a frequency of $f_2 H/U_0 = 0.12$, still another at the frequency of $f_3 H/U_0 = 0.24$, and a distant peak at the frequency of $f_4 H/U_0 = 1.28$. The highest frequency peak matches the Kelvin–Helmholtz frequency of the mixing layer, and is associated with modes 68 and 69. Fig. 4 confirms that this frequency corresponds to mixing layer modes (which is particularly clear for mode 69).

We believe the two lowest frequencies to be associated with the recirculation bubble (the third frequency $f_3 H/U_0 = 0.24$ is simply likely to be a harmonic of $f_2 H/U_0 = 0.12$). The lowest frequency $f_1 H/U_0 = 0.04$–0.05 can be seen to correspond to the flapping frequency which is associated with the growth and shrinkage of the bubble [7]. If this frequency is renormalized with the recirculation length, we find an adimensional frequency of $fL_R/U_0 = 0.12$ which matches results in the literature [1]. We note that this frequency corresponds to the circulation time scale associated with the main vortex inside the recirculation bubble.

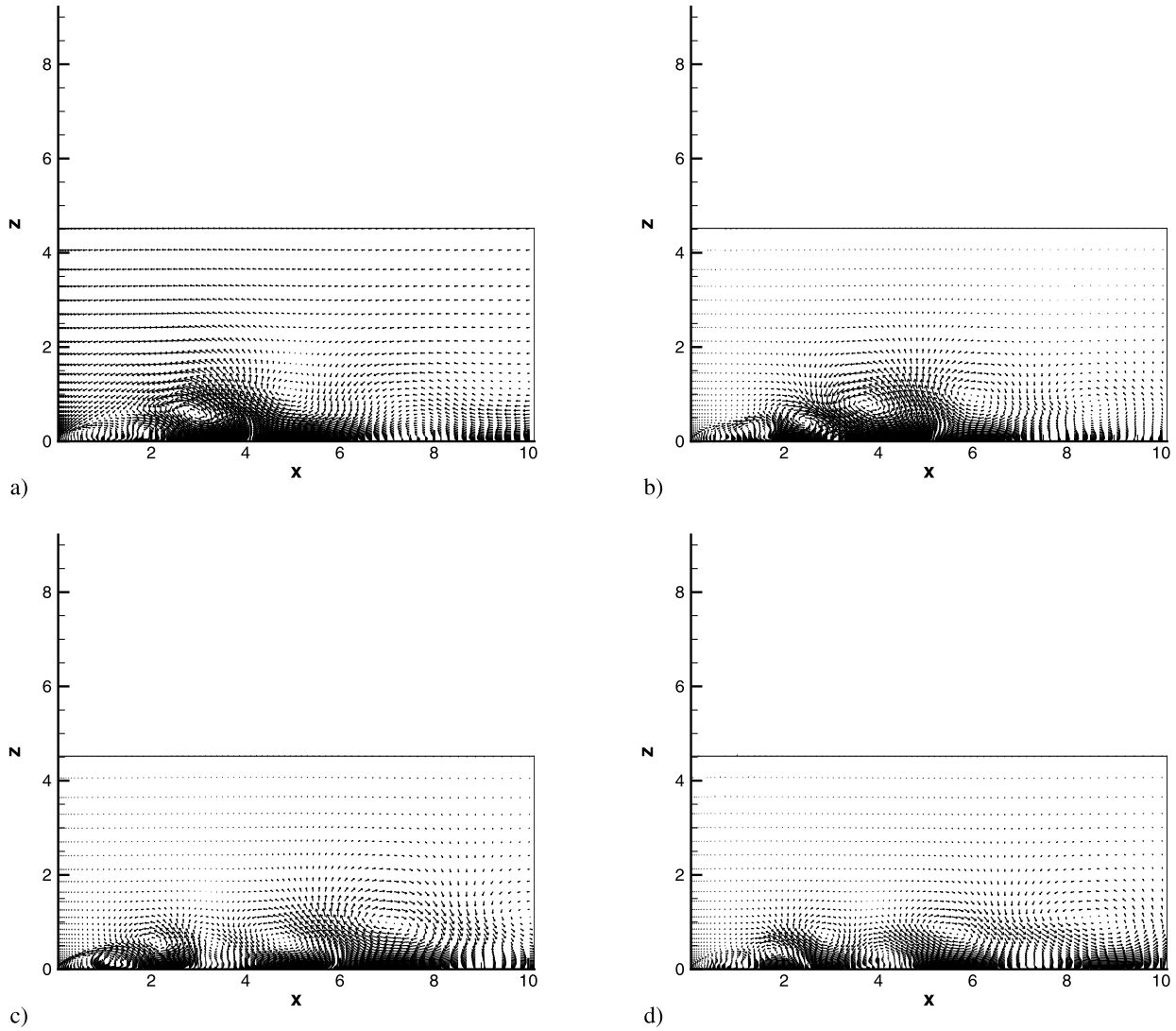

Fig. 8. Pressure-educed spanwise-averaged velocity mode: a) $n = 2$, b) $n = 3$, c) $n = 4$, d) $n = 5$.

The other frequency does not match Kiya et al.'s results if we normalize it with our recirculation length. However it matches their value if the frequency is rescaled with the thickness of the plate. It is generally agreed that the vortex shedding process corresponds to a Karman instability [8] in which the vortices interact with the wall, which creates by reflection a row of aligned vortices (not staggered, unlike a classical vortex street) of opposite sign [9]. The frequency should therefore scale with the vertical distance between the vortex and the wall, which depends on the bubble height, while the flapping frequency is associated with the recirculation time scale within the bubble, and therefore depends on the recirculation length.

All modes $n \leq 10$ contain both the shedding and the flapping frequencies – it was not possible to separate both contributions in any of the modes (which could be done using Fourier transform or equivalently DMD decomposition). This coupling supports the idea of a single physical origin for the two different frequencies observed. Although both flapping and shedding can be viewed as primarily two-dimensional processes, the structure of the flow is strongly three-dimensional, as illustrated in Fig. 5 by a horizontal section of the most energetic fluctuating mode. A characteristic spanwise scale of $L_y/3 \sim 1.3H$ can be identified beyond the reattachment point.

3.3. Surface pressure POD

POD analysis was also applied to the surface pressure along the plate. The pressure spectrum is shown in Fig. 2b. As could be expected, since the domain is limited to a plane and only one scalar is considered, the convergence of the spectrum is faster. The first two modes are nearly equal, which suggests the presence of a spatio-temporal symmetry. The spectral

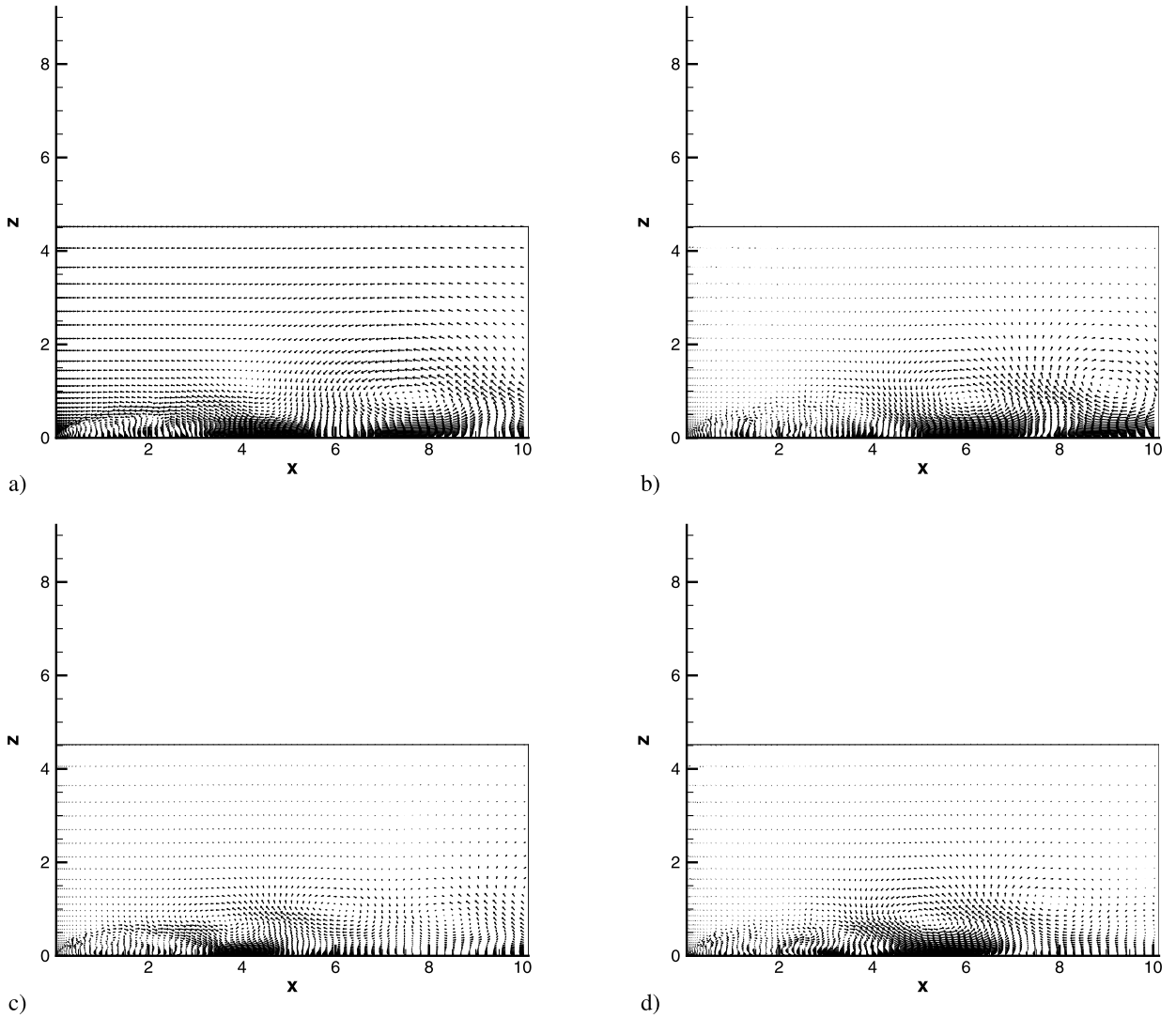

Fig. 9. Spanwise-averaged full POD velocity mode: a) $n = 2$, b) $n = 3$, c) $n = 4$, d) $n = 5$.

content of the POD pressure modes can be seen to be very similar to that of the full field counterparts. Higher-order modes are associated with higher frequencies, with a significant low-frequency contribution observed in the first 100 modes of the field (Fig. 6a). In the first POD pressure modes, two main frequencies could be identified, which correspond to the flapping and shedding frequencies observed for the POD velocity modes, as is shown in Fig. 6b). For the first ten modes, a peak is present at $fH/U_0 = 0.05$, and a second one at $fH/U_0 = 0.13$, with a significant content in the range $[0.13, 0.17]$. The Kelvin–Helmholtz frequency does not appear in the pressure spectrum. Fig. 7 shows the first four fluctuating POD pressure modes. It is clear that the two most energetic fluctuating modes are mostly invariant in the spanwise direction, as was argued by Peter Jordan (private communication). The idea that the wall pressure fluctuations constitute the signature of vortices is supported by application of the extended POD. The extended POD velocity modes based on the pressure were computed, using the technique first put forth by Borée [10]. If the n-th pressure mode Φ_p^n can be written as

$$\Phi_p^n(x, y) = \sum a_p^n(t^m)\, p(x, y, t^m) \tag{4}$$

where $p(x, y, t^m)$ is the pressure field at the instant t^m, the corresponding extended velocity mode can be obtained from

$$\underline{\Phi}_{u(p)}^n(x, y, z) = \sum a_p^n(t^m)\, \underline{u}(x, y, z, t^m) \tag{5}$$

Since the pressure is constant in the spanwise direction (at least for the highest two fluctuating modes), it makes sense to look at the spanwise average of the extended velocity modes, which are represented in Fig. 8. The first two fluctuating modes consist of a strong vortex centered above the reattachment point and convected outside the recirculation bubble. This

is in full agreement with the observations of Tung [11]. The next two modes consist of two same-sign vortices located on either side of the mean reattachment point at a distance $x = 2H$ and $x = 4.2H$ from the edge of the plate. A counter-rotating vortex can be observed between these vortices.

The corresponding spanwise average of the POD velocity modes is represented for comparison in Figs. 9 with the same scale. One vortex is observed for the first fluctuating mode at $x = 8H$ from the edge of the plate. The second mode contains a pair of unequal counter-rotating vortices with centers at a distance $x = 6H$ and $x = 8H$ from the edge of the plate. Respectively three and two vortices can be identified for fluctuating modes 3 and 4.

The vortical motions associated with the velocity POD modes are less intense than the ones associated with the pressure-educed structures.

4. Conclusion

POD analysis of the flow along a flat thick plate shows that the most energetic motions consist of large-scale vortices shed behind the recirculation bubble. The spanwise extent of these vortices is of order H and their separation is about $2H$, where H is the plate's thickness. The motions are characterized by two frequencies $fH/U_0 = 0.04$ and $fH/U_0 = 0.12$, which are associated with the flapping of the recirculation bubble, and the shedding process. POD analysis of the surface pressure shows that the pressure modes are quasi-invariant in the spanwise direction. The vortical motions associated with the pressure modes are obtained by EPOD and are found to be most intense in the reattachment region.

References

[1] M. Kiya, K. Sasaki, Structure of large-scale vortices and unsteady reverse flow in the reattaching zone of a turbulent separation bubble, J. Fluid Mech. 154 (1985) 463–491.
[2] C. Tenaud, Y. Fraigneau, V. Daru, Numerical simulation of the turbulent separation reattachment flow around a thick flat plate, in: Proceedings of ETC, vol. 13, 2011.
[3] M. Germano, U. Piomelli, P. Moin, W. Cabot, A dynamic subgrid-scale eddy-viscosity model, Phys. Fluids A 3 (1991) 1760.
[4] P. Holmes, J.L. Lumley, G. Berkooz, Turbulence, Coherent Structures, Dynamical Systems and Symmetry, Cambridge University Press, Cambridge, UK, 1996.
[5] L. Sirovich, Turbulence and the dynamics of coherent structures. Part I: Coherent structures, Q. Appl. Math. 45 (3) (1987) 561–571.
[6] B. Podvin, P. Le Quéré, Low-order p.o.d.-based models for the flow in a differentially heated cavity, Phys. Fluids 13 (2001) 3204–3214.
[7] A. Fouras, J. Soria, Large scale flapping of separated flow, in: Proceedings of the 13th Australasian Fluid Mechanics Conference, December 1995.
[8] A. Roshko, On the wake and drag of bluff bodies, J. Aeronaut. Sci. 22 (1955) 124–132.
[9] L.W. Sigurdson, The structure and control of turbulent reattaching flow, J. Fluid Mech. 298 (1995) 205–234.
[10] J. Borée, Extended proper orthogonal decomposition: a tool to analyse correlated events in turbulent flows, Exp. Fluids (2003) 188–192.
[11] T.T. Tung, Modélisation hybride RANS/LES d'écoulements massivement décollés en régime turbulent. Études des corrélations pression/vitesse et confrontation à l'expérimentation, PhD thesis, Université de Poitiers, Poitiers, France, 2012.